Comprehensive Model for the Thermoelectric Properties of Two-Dimensional Carbon Nanotube Networks

Aditya Dash, Dorothea Scheunemann⬤, and Martijn Kemerink⬤[*]

Institute for Molecular Systems Engineering and Advanced Materials, Heidelberg University, Im Neuenheimer Feld 225, 69120 Heidelberg, Germany

Networks of semiconducting single-walled carbon nanotubes (SWCNTs) are interesting thermoelectric materials due to the interplay between CNT and network properties. Here, we present a unified model to explain charge and energy transport in SWCNT networks. We use the steady-state master equation for the random resistor network containing both intra- and intertube resistances, as defined through their one-dimensional density of states that are modulated by static Gaussian disorder. The tube-resistance dependence on the carrier density and disorder is described through the Landauer formalism. Electrical and thermoelectric properties of the network are obtained by solving Kirchhoff's laws through a modified nodal analysis, where we use the Boltzmann-transport formalism to obtain the conductivity, Seebeck coefficient, and electronic contribution to the thermal conductivity. The model provides a consistent description of a wide range of previously published experimental data for temperature and charge-carrier-density-dependent conductivities and Seebeck coefficients, with energetic disorder being the main factor to explain the experimentally observed mobility upswing with carrier concentration. Moreover, we show that, for lower disorder energies, the Lorentz factor obtained from the simulation is in accordance with the Wiedemann-Franz law for degenerate-band semiconductors. At higher disorder, deviations from simple band behavior are found. Suppressed disorder energy and lattice thermal conductivity can be the key to higher thermoelectric figures of merit, zT, in SWCNT networks, possibly approaching or even exceeding $zT = 1$. The general understanding of transport phenomena will help the selection of chirality, composition, and charge-carrier density of SWCNT networks to improve their efficiency of thermoelectric energy conversion.

I. INTRODUCTION

Since the seminal work of Hicks and Dresselhaus in the 1990s [1,2], which, on basis of theoretical considerations, showed that a significant increase in the thermoelectric figure of merits, zT (see Sec. II), can be achieved by going to lower dimensionalities, research interest in carbon nanotubes as thermoelectric materials has increased considerably. As a one-dimensional (1D) material with a corresponding density of states, it offers, besides stability, flexibility, and solution processability, a unique combination of properties, such as high carrier mobilities and high Seebeck coefficients, which makes it attractive for thermoelectric applications. Theoretical models for individual nanowires (NWs) show that the Seebeck coefficient and band gap can be tuned via the tube diameter, allowing Seebeck coefficients larger than 2000 $\mu V\,K^{-1}$ to be achieved at tube diameters of 0.6 nm [3–5]. Moreover, single-walled carbon nanotube (SWCNT) networks can also achieve high conductivity values as soon as they are

doped appropriately [6,7]. Since both the Seebeck coefficient and the conductivity are sensitive to the position of the Fermi energy, and thus, the carrier density, attempts have been made to experimentally find the optimal carrier density for a maximum zT factor, using gate-contact-based transistors [8,9].

However, a fundamental understanding of the underlying physics of charge and energy transport in networks of nanotubes is still missing but required to rationally improve the performance of such systems at the lowest possible cost. Combining the knowledge gained from research on single nanowires with general network properties allows, in principle, the modeling of entire three-dimensional NW networks with different densities and compositions, including the corresponding electrostatics. However, this task is extremely complex, so that two-dimensional (2D) networks are often used as a testbed, where information about current paths and energy transport is already accessible.

Various models, such as fluctuation-induced tunneling, variable-range hopping, and percolation theory, have been used to fit mobility data of NW networks; however, they

---

*martijn.kemerink@cam.uni-heidelberg.de

do not directly provide conclusions on the microscopic transport mechanism [10–14]. In addition, there are some studies that simulate the conductivity of two- or three-dimensional NW networks based on random resistor networks, but only a few include intrinsic properties of NWs, such as the one-dimensional density of states (DOS), and take into account the carrier-density dependence of the transport properties [15].

Schießl *et al.* used a random-resistor model of SWC-NTs considering the DOS and junction resistance of individual NWs to model the charge-density dependence of the field-effect mobilities of mixed-chirality SWCNT networks [16]. Unfortunately, a small numerical error in the model (see Sec. II) affected some of the results, causing a mobility versus carrier-density peak even at zero disorder energy. No other thermoelectric parameters, such as the Seebeck coefficient or thermal conductivity, were calculated. The tube resistance was not considered. In contrast, Statz *et al.* investigated, both experimentally and by means of modeling, the temperature and carrier-density dependence of the mobility and Seebeck coefficient [17]. However, the authors do not use a single consistent model to describe the data but instead use fluctuation-induced tunneling and Boltzmann-transport formalisms to describe the mobility and the Seebeck coefficient, respectively. In summary, there is, to date, no model that can simultaneously and consistently describe the electrical conductivity, the electronic contribution to the thermal conductivity, and the Seebeck coefficients of SWCNT networks.

Here, we model a quasi-2D resistor network considering the intra- and intertube resistances based on the Landauer formalism and the steady-state master-equation approach, respectively [18,19]. This successfully reproduces the mobility versus carrier-density peak, which is a key characteristic of the experiments, in terms of percolation in an energetically disordered medium. We use the Boltzmann-transport equation (BTE) to extend the model to find the Seebeck coefficient and the electronic contribution to thermal conductivity. As such, we obtain a unified model that consistently reproduces the experimental thermoelectric factors and that can be used to identify optimal parameter values to obtain high-zT factors in general quasi-2D SWCNT networks.

II. MODEL

In this work, we model the electronic and thermoelectric properties of SWCNT networks as a heterogeneous resistor network in combination with the Boltzmann-transport formalism. The model accounts for both the intratube resistance and the intertube or junction resistances. From experiments, it is commonly understood that the former (tube) resistance is lower by 1–4 orders of magnitude than the latter (junction) resistance, which, so far, has motivated

the exclusion of the former in charge-transport modeling [20–26]. Our model essentially extends these works, and particularly that of Schießl, who solved the steady-state master equation, accounting for junction conductances in a monodisperse SWCNT system with Gaussian energetic disorder, to also account for tube resistances [16]. It is shown below that the latter have a notable influence on measured conductivities. Moreover, we calculate thermoelectric factors like the Seebeck coefficient and the (electronic part of the) thermal conductivity of the network.

The simulation starts by creating a random resistor network, where the SWCNTs are treated as 1D wires that are randomly dispersed in the 2D calculation box of size $L_x \times L_y$ with periodic boundary conditions as visualized in Fig. 1(a). The network density is characterized by linear density l_d, while nanotube lengths l_i are drawn from a normal distribution with mean l_0 and width σ_l to replicate the tube-length variations in the experiment, as obtained from, e.g., atomic force microscopy. The total number of tubes dispersed in the box then becomes

$$N_T = \frac{l_d \cdot L_x \cdot L_y}{l_0}. \quad (1)$$

The density of states, $g(E, E_c)$, with E_C as the conduction-band edge of a given type of CNT, is parametrized on the basis of the results from Ref. [27], which reports nearest-neighbor tight-binding calculations, including the trigonal wrapping effects. Energetic disorder, which, among others, can result from defects and (charged) impurities in both the CNT film and the substrate, is implemented in the network as a Gaussian distribution of conduction-band-edge energies of the individual tubes with width σ_{DOS}. Hence, each SWCNT i is assigned a DOS $g(E, E_{c,i})$, where $E_{c,i}$ are selected from a Gaussian distribution with mean E_c and standard deviation σ_{DOS}, see Fig. S6 within the Supplemental Material [28].

The charge-carrier density of the network is determined by summation of the carrier density in the individual tubes within the box area:

$$n(E_F) = \frac{\beta}{L_x \cdot L_y} \sum_i^{N_T} \int_{E_{c,i}}^{\infty} l_i \cdot g(E, E_{c,i}) \cdot f_d(E, E_F) dE, \quad (2)$$

where l_i is the length of SWCNT i, E_F is the Fermi energy, and β is the SWCNT bundling factor, as illustrated in Fig. 1(d) [29]. The occurrence of bundled SWCNTs in the experiment would cause an underestimation of the network density, and concomitantly of the carrier density, if they were treated as a single SWCNT in the model; the beta factor is used for scaling up to the experimental carrier density in the model.

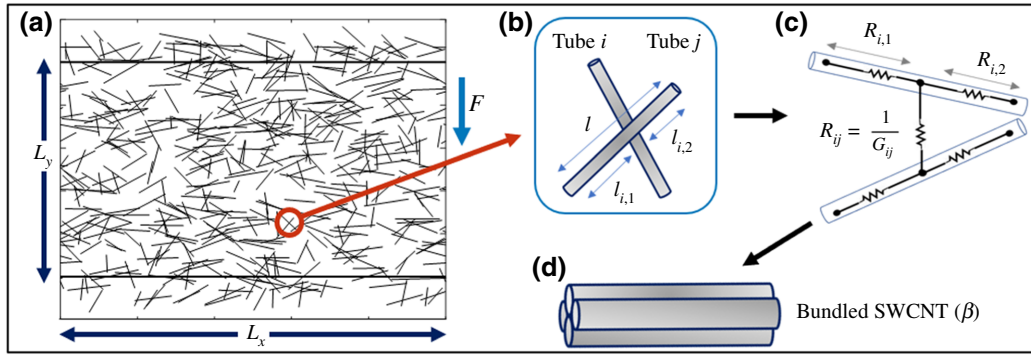Considering charge transport within the tube junction as a disordered system, the Miller-Abrahams

FIG. 1. Outline of the numerical model. (a) 2D SWCNT network consisting of randomly dispersed 1D tubes of linear density l_d and mean length l_0. Fat horizontal lines are source and drain contacts. (b) Magnification of a single junction, which divides tubes i and j into two segments each, leading to (c) resistor (sub)network. (d) Aggregated SWCNTs may form bundles in the network, which is accounted for by a bundling factor, β.

hopping formalism is introduced into the steady-state master equation, where the occupation probability of different sites is calculated through the Fermi-Dirac distribution [30]. The mean-field method in the low-electric-field approximation solves the set of master equations, leading to the junction conductance:

$$G_{ij}(E_F, E_i, E_j) = \int_{E_{c,i}}^{\infty} \int_{E_{c,j}}^{\infty} \frac{e^2 \omega_{ij}^*(|\Delta E_{ij}|)}{4 k_B T \cosh\left(\frac{E_i - E_F}{2 k_B T}\right) \cosh\left(\frac{E_j - E_F}{2 k_B T}\right)} g(E_i, E_{c,i}) g(E_j, E_{c,j}) dE_i dE_j, \tag{3}$$

where ΔE_{ij} is the difference between energy states E_i and E_j, e is the electronic charge, k_B is the Boltzmann constant, and $\omega_{ij}^* = \omega_0 exp(-|\Delta E_{ij}|/2k_B T)$ is the symmetric hopping rate with ω_0 an attempt to hop rate, see Fig. 1(b) [31–33]. The symmetric form of ω_{ij}^* avoids the directional dependence of the node conductance in the 2D resistor network [34].

The intratube (segment) resistance is formulated based on the extension to the Landauer formula:

$$R_s = \frac{h}{4e^2}\left(1 + \frac{l_0}{L_F}\right), \tag{4}$$

accounting for the length-dependent carrier-transmission rate [35]. If the mean tube length, l_0, is comparable to the Fermi length, L_F, the system is in the ballistic regime; otherwise, the classical limit of the diffusive regime holds. L_F is then related to the carrier density of the tube using Fermi's golden rule and scattering analysis for acoustic phonons. In SWCNTs, transport along the tube direction can be calculated from acoustic phonon scattering in a 1D relativistic band structure as

$R_{i,k}$

$$= \frac{h}{4e^2}\left(1 + \frac{\alpha l_{i,k} T}{v_0 d}\left(1 + \left(\frac{8}{3 \cdot \pi \cdot \eta(E_{c,i}, E_F) \cdot l_{i,k}}\right)^2\right)\right), \tag{5}$$

where v_F is the Fermi velocity, d is the SWCNT diameter, $\eta(E_{c,i}, E_F)$ equals the carrier density of the individual SWCNT, and α relates the scattering events to the acoustic phonons [36,37]. An α value of 6.5 m/Ks is taken for all calculations [38]. Moreover, $l_{i,k}$ is the length of nodal segment k of SWCNT i, see Fig. 1(b). The total number of nodal segments in tube i equals $N_i = n_i + 1$, where n_i is the total number of the junctions in the tube.

Once the individual resistance values are obtained from semiclassical Eqs. (3) and (5), the classical equivalent resistance network is established, as depicted in Fig. 1(c). Although the individual elements in the disordered network may show quantum mechanical behavior around room temperature, it is not to be expected that wavefunction coherence exists beyond the smallest length scales in the network under these conditions. Hence, the constituent elements in the network can be treated as independent, that is, by using the corresponding (semiclassical) resistance values as Ohmic elements in a classical network simulation [15,23].

A small voltage, V, is applied between the electrodes and a modified nodal analysis is used to solve the coupled Kirchhoff equations, obtaining all segment currents and the overall current, I_n, in the network. The total 2D network conductivity, σ_n, is then calculated as

$$\sigma_n = \frac{I_n}{V}\frac{L_y}{L_x^2}, \tag{6}$$

which thus incorporates both the tube and junction behavior.

Following Fritzsche, the Seebeck coefficient can be calculated from the Boltzmann-transport formalism as

$$S = \frac{-k_B}{e} \int \left(\frac{E - E_F}{k_B T}\right) \frac{\sigma'(E, E_F)}{\sigma} dE$$

$$= \frac{-k_B}{e} \int \left(\frac{E - E_F}{k_B T}\right) \frac{I(E, E_F)}{I} dE, \qquad (7)$$

where $\sigma'(E, E_F)$ is the conductivity distribution function for a given value of E_F, $\sigma(E, E_F)$, times the derivative of the Fermi-Dirac distribution, df_D/dE [4,39,40]. In the second equality, the dependency on σ' is transformed into one on the energy-dependent current distribution function, $I(E, E_F)$, by multiplying the numerator and denominator with the field, $F = V/L_y$, which is numerically easily accessible, in contrast to $\sigma(E, E_F)$.

Due to the van Hove singularity at the band edge of the 1D DOS, the majority contribution to $I(E)$ comes from the band edge, leading to

$$I(E, E_F) \propto I_{i,k}(E_F)\delta(E - E_{c,i}), \qquad (8)$$

where $I_{i,k}$ is the current in nodal segment k of SWCNT i. Substituting Eq. (8) into Eq. (7), while including the length dependence of the nodal segments, leads to

$$S_C = \frac{\frac{-k_B}{e} \sum_i^{N_T} \sum_k^{N_i} \int_{E_{c,i}}^{\infty} \left(\frac{E - E_F}{k_B T}\right) I_{i,k}(E_F) \cdot l_{i,k}\delta(E - E_{c,i})dE}{\sum_i^{N_T} \sum_j^{N_i} I_{i,k}(E_F)l_{i,k}},$$

$$= \frac{\frac{-k_B}{e} \sum_i^{N_T} \sum_k^{N_i} \left(\frac{E_{c,i} - E_F}{k_B T}\right)\omega_{i,k}}{\sum_i^{N_T} \sum_k^{N_i} \omega_{i,k}}, \qquad (9)$$

where $\omega_{i,k} = I_{i,k}(E_F) \cdot l_{i,k}$ is the weighting factor of the current contribution based on the segment length.

To obtain the contribution A to the thermopower due to near-band-edge states, the current distribution function can be approximated as

$$I(E, E_F) \propto g(E, E_c)\left(\frac{-\partial f_D}{\partial \varepsilon}\right). \qquad (10)$$

Similarly, substituting Eq. (10) into Eq. (7), the remaining DOS contribution to S can be calculated as

$$A = \frac{\frac{-k_B}{e} \sum_i^{N_T} \sum_k^{N_i} \int_{E_{c,i}}^{\infty} \left(\frac{E - E_{c,i}}{k_B T}\right) \omega_{i,k} g(E, E_{c,i})\left(\frac{-\partial f_D}{\partial \varepsilon}\right) dE}{\sum_i^{N_T} \sum_k^{N_i} \int_{E_{c,i}}^{\infty} \omega_{i,k} g(E, E_{c,i})\left(\frac{-\partial f_D}{\partial \varepsilon}\right) dE}. \qquad (11)$$

The total Seebeck coefficient for the SWCNT network then becomes

$$S = S_C + A. \qquad (12)$$

For charge and energy transport occurring in disorder-dominated systems, which is shown to be the case for the SWCNT systems discussed herein, the Seebeck coefficient can quasi-quantitatively be understood by a simple expression that is based on the notion that S equals the entropy carried out by a unit charge [41]:

$$S \approx -\frac{E_t - E_F}{k_B T}. \qquad (13)$$

Here, E_t is the transport energy that can be defined in the context of percolation theory as the characteristic energy of the final (hopping) state, E_j, which is largely independent of initial site energy, E_i [42,43]; for the typical value of the latter, the Fermi energy is used. Equation (13) is not used

for calculation purposes but is used in later discussions for explanatory purposes.

The electronic contribution to the thermal conductivity under open-circuit conditions, κ_0, is similarly formulated from the Boltzmann-transport formalism. The theoretical macroscopic description of the electronic thermal conductivity is then obtained from [44]

$$\kappa_{\text{el}} = \kappa_0 - S^2 \sigma T. \qquad (14)$$

As for S, κ_0 can be split into two components: a band-edge-dependent contribution,

$$K_{\text{ec}} = \frac{\frac{-k_B}{e}\sigma_n \sum_i^{N_T} \sum_k^{N_i} \left(\frac{(E_{c,i} - E_F)^2}{k_B T}\right) \omega_{i,k}}{\sum_i^{N_T} \sum_k^{N_i} \omega_{i,k}}, \qquad (15)$$

and a contribution from near-band-edge states,

$$A_{\text{ec}} = \frac{\frac{-k_B}{e}\sigma_n \sum_i^{N_T} \sum_k^{N_i} \int_{E_{c,i}}^{\infty} \left(\frac{(E-E_{c,i})^2}{k_B T} \right) \omega_{i,k} g(E,E_{c,i}) \left(\frac{-\partial f_D}{\partial \varepsilon} \right) dE}{\sum_i^{N_T} \sum_k^{N_i} \int_{E_{c,i}}^{\infty} \omega_{i,k} g(E,E_{c,i}) \left(\frac{-\partial f_D}{\partial \varepsilon} \right) dE}. \tag{16}$$

The thermoelectric figure of merit, zT, which is a measure of a material's efficiency of thermoelectric power conversion, can now be expressed in terms of the above-defined parameters as

$$zT = \frac{\sigma S^2 T}{\kappa}, \tag{17}$$

where κ is the total thermal conductivity, $\kappa = \kappa_{\text{el}} + \kappa_{\text{latt}}$, with κ_{latt} as the lattice thermal conductivity and σ as the three-dimensional (3D) conductivity, which can be estimated from the 2D network conductivity, σ_n, by dividing by the (estimated) film thickness.

Although the model outlined above is applicable to any single or mixed chiral composition SWCNT network, we consider the (6,5) chiral SWCNT for the following calculations.

III. RESULTS AND DISCUSSION

Since the presence of energetic disorder will turn out to be central to understanding the reported experimental observations in SWCNT networks, we first investigate the (normalized) mobility versus charge-carrier density for systems with different disorder. Figure 2(a) shows that for small disorder, $\sigma_{\text{DOS}} < k_B T$, the mobility rolls off with increasing Fermi energy, that is, towards higher charge-carrier densities. This behavior can directly be understood in terms of Eq. (3), which, in the absence of disorder

$(E_i = E_j)$ predicts a slightly weaker increase in conductivity than in carrier density. For larger disorder values, a characteristic mobility maximum develops, see also the inset to Fig. 2(a). Similar behavior is well known for disordered organic semiconductors, where increasing mobility reflects the Fermi energy moving towards the transport energy, E_t [45,46]. The high-density mobility (μ) roll-off occurs for the same reason as that at low disorder. Although we consider only homogeneous SWCNT networks here, we note that, for mixed chiral networks, the peaked mobility is already observed for lower disorder values, due to the tube species with the lowest band-edge energies acting as trap states that have a similar effect to that of energetic disorder.

In Fig. 2(b), we compare our model to experimental data from Rother *et al.*, using a modest energetic disorder of 60 meV. The model provides an accurate description of the experiment. The blue line, which is the best reported fit by Schießl and co-workers, shows a broadened mobility peak with a mobility minimum prior to the onset. Both features are due to a numerical problem in the implementation used in Ref. [16], which is associated with the limits of the double integration needed to obtain G_{ij} in the presence of a van Hove singularity at the band edge. The steeper mobility increase with carrier density for the calculation in which the tube resistance is neglected (red line) signifies the importance of the tube resistance to overall charge transport. This also provides us with a general sense of what
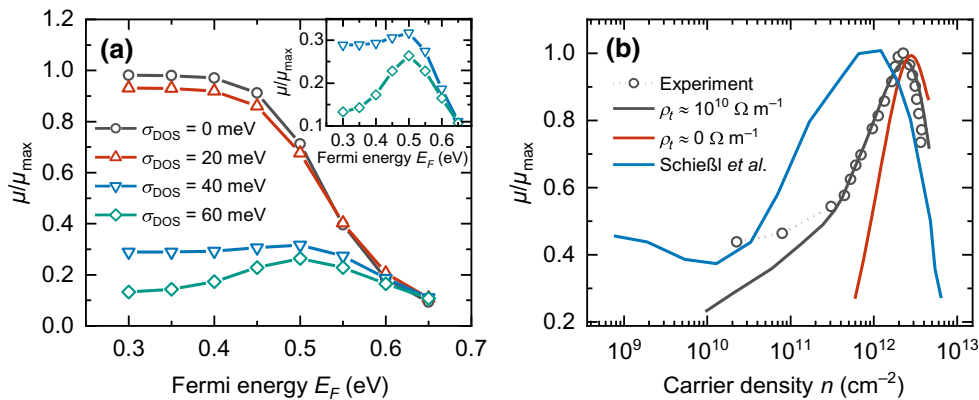

FIG. 2.   Calculated normalized mobility using mobility maxima (μ_{max}) for (6,5) chiral SWCNT networks: (a) versus Fermi energy, parametric in energetic disorder (inset is a magnification of the development of the mobility peak at higher disorder), $l_0 = (1.5 \pm 0.6)\ \mu\text{m}$, $l_d = 7\ \mu\text{m}^{-1}$; (b) versus 2D charge-carrier density, compared with experimental data from Ref. [47] measured in field-effect-transistor geometry (symbols) and the best fit from Ref. [47] (blue line). Black line is for the full model; the value for ρ_t in the legend is the approximate numerical value for the tube resistivity; the red line is for $\rho_t = 0$. Linear density of the network is $l_d = 30\ \mu\text{m}^{-1}$ with mean tube length $l_0 = 1\ \mu\text{m}$, dispersion $\sigma_l = 0.3\ \mu\text{m}$, and $\beta = 1$.
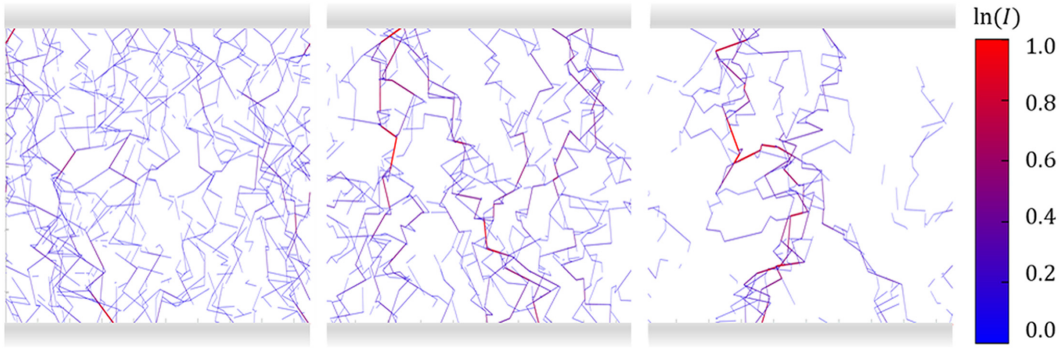
FIG. 3. Current distribution in the SWCNT network with varying disorder at constant Fermi energy, $E_F = 0.5$ eV. Cutoff $I_{cut} = 0.05 \times I_{max}$, where I_{max} is the maximum current carried by a single tube segment in the network, is applied to prevent the low-current-carrying tubes in the network from dominating the image. Disorder $\sigma_{DOS} = 0, 90,$ and 180 meV from left to right; otherwise, same parameters as in Fig. 2(a) are used.

mobility versus carrier-concentration curves in Ref. [16] would resemble when the numerical error is corrected.

In Fig. 3, the evolution of the percolation paths in the SWCNT network is shown for increasing disorder for constant $E_F = 0.5$ eV. A distinct percolation path for charge transport can be seen at a relatively high disorder, whereas a relatively low disorder leads to a more distributed current path in the network. This behavior is consistent with the notion that percolation phenomena, including the occurrence of a mobility maximum at a well-defined carrier density, cf., Fig. 2, become more important at increased energetic disorder. Specifically, the homogeneous network in the left panel of Fig. 3 is not expected to respond critically upon more tubes becoming energetically available due to the Fermi level moving up, that is, upon increasing the carrier density, cf., Eq. (3). In other words, the network mobility remains essentially constant until the

roll-off discussed in the context of Fig. 2(a) sets in. In contrast, in the more critical network that forms for higher disorder (right panel), making further tubes accessible by increasing the charge carrier density will have a superlinear effect on the conductivity, and hence, lead to an increasing mobility.

Having established that neither energetic disorder nor the intratube resistance can be ignored in 2D SWCNT networks, we address the simultaneous description of charge and energy transport in said systems. Figure 4 shows the temperature dependence of combined mobility and Seebeck coefficient measurements on (6,5) chiral SWCNT networks taken from Ref. [17].

For bundling factor $\beta = 4.3$ and $\sigma_{DOS} = 110$ meV, the model provides a reasonably accurate description of both experiments, as depicted in Figs. 4(a) and 4(b). We note that experimental data result from separate
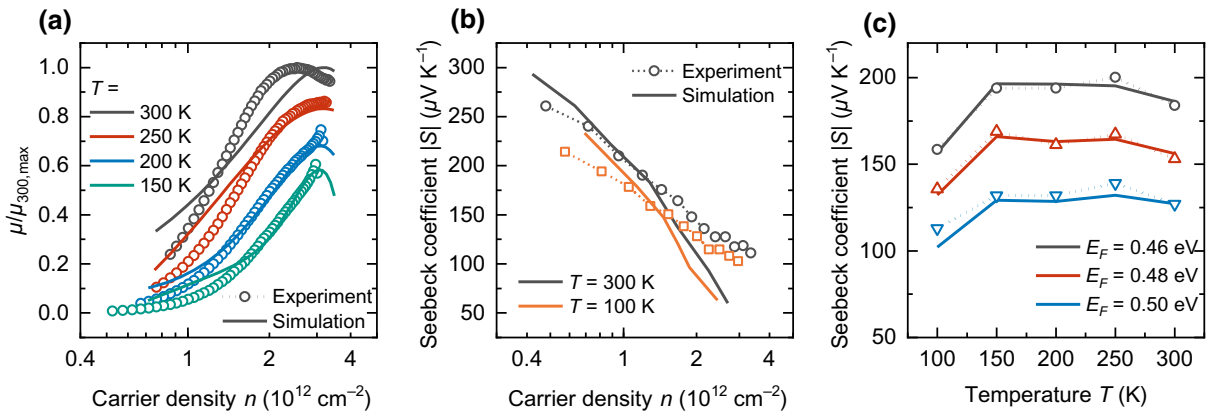

FIG. 4. Simultaneous fit to the temperature dependence of mobility (a) and Seebeck coefficient (b) of (6,5) chiral SWCNT networks. Experimental data are measured in field-effect-transistor geometry and are taken from Statz *et al.* [17]. Linear density of the network is $l_d = 12.6$ μm^{-1} with mean tube length $l_0 = (0.95 \pm 0.4)$ μm. (6,5) SWCNT networks are treated with 1,2,4,5-tetrakis(tetramethylguanidino)benzene (TTMGB), which leads to pure electron transport. Key simulation parameters are given in the legends. Moreover, $\sigma_{DOS} = 110$ meV, $\beta = 4.3$. (c) Fit to S versus T only for $\sigma_{DOS} = 92$ meV and $\beta = 7$. Carrier density corresponding to E_F mentioned in the caption, $n = 1.29 \times 10^{12}, 1.83 \times 10^{12},$ and 2.54×10^{12} cm^{-2}, going from lower to higher E_F. ($\mu_{300,max}$ refers to the mobility maxima at 300 K.)
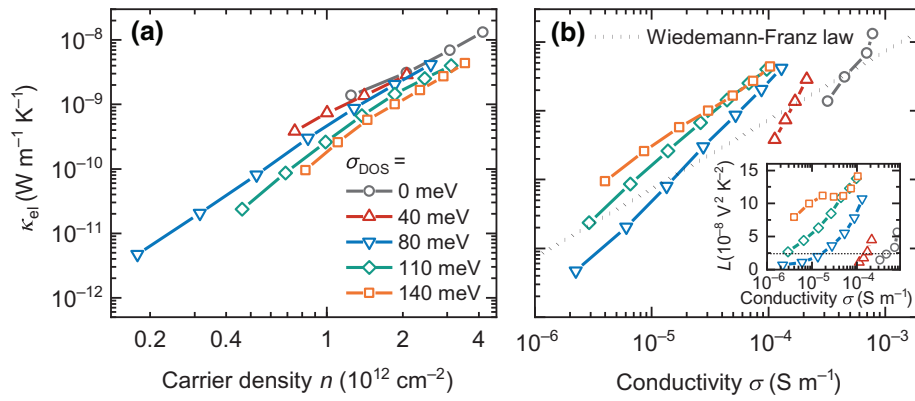
FIG. 5.   Electronic contribution to thermal conductivity from the numerical model for various energetic disorder values versus (a) carrier concentration and (b) conductivity. Inset in (b) shows the effective Lorentz factor, L, as defined through the Wiedemann-Franz (WF) law. Parameters used are $\beta = 4.3$, $l_d = 12.6 \ \mu\text{m}^{-1}$, and $l_0 = (0.95 \pm 0.4) \ \mu\text{m}$.

measurements on nominally identical devices, concomitantly, closer matching fits can be produced if we allow slightly different parameters for the mobility and Seebeck measurement data, see Fig. S3 within the Supplemental Material [28] and Fig. 4(c). A closer look in experimental data from Ref. [17] reveals that, for a given carrier density, the Seebeck coefficient is mostly temperature independent to about 150 K, below which it drops. In Fig. 4(c), for a slightly relaxed $\sigma_{\text{DOS}} = 92$ meV, we present model fits to three such traces taken at different carrier concentrations. The observed behavior, and possibly even fluctuations at higher temperatures, can be consistently captured by the model. The sudden drop in S at lower T occurs only at higher energetic disorder and results from the interplay between (the temperature dependence of) all terms in Eq. (13) and coincides with an increased temperature dependence of the transport energy, E_t, at lower T; at higher temperatures, the T dependence of the terms in the numerator, $E_t - E_F$, largely compensate for the linear T dependence of the denominator. Figs. S4(a) and S4(b) within the Supplemental Material [28] further elaborate on this topic.

In Ref. [17], the temperature dependence of mobility is described with a fluctuation-induced tunneling model, which provides no natural explanation for the peak in the mobility versus density, and is based on fundamentally different assumptions from those in the model proposed by Schießl *et al.* [16] to explain similar data. Seebeck data are interpreted using a Boltzmann-transport model with low ($\sim$8 meV) energetic disorder, which leads to a more gradual temperature dependence than that found in Fig. 4(c). The modeling results presented in Figs. 2 and 4 show that it is possible to provide a consistent description of (thermo)electric measurements on SWCNT networks using an extended hopping model with significant disorder.

The finding that a significant amount of energetic disorder affects the systems' physical properties should

come as no surprise, since experimental data are obtained on field-effect-transistor (FET) devices. From similar measurements on organic FETs, it is known that the gate dielectric induces an energetic disorder of several times the thermal energy in the accumulation layer [48,49]. For data in Fig. 4, an additional contribution to the energetic disorder, σ_{DOS}, may be expected due to treatment with strongly reducing TTMGB [17].

Having established the applicability of the model, we now turn to the related question of heat transport, that is, the electronic contribution to the thermal conductivity, $\kappa = \kappa_{\text{el}} + \kappa_{\text{latt}}$, which is the denominator of zT, Eq. (17). Hence, a quantitative analysis of heat-transport phenomena is an important factor for assessing the applicability of CNT networks for thermoelectric applications. In Fig. 5, the electronic thermal conductivity can be seen to roughly follow the Wiedemann-Franz law:

$$\kappa_{\text{el}} = LT\sigma,$$

with L as the Lorentz number, which is typically close to the Sommerfeld value, $L_0 = \pi^2/3(k_B/q)^2$ [44]. The decrease in κ_{el} with increasing disorder at constant density, cf., Fig. 5(a), therefore, predominantly reflects a lower conductivity, σ. In fact, (the inset in) Fig. 5(b) shows that, with increasing disorder, the Lorentz number actually increases from a value that is close to or even below L_0 to considerably larger values. A similar increase in L with disorder is found for doped organic semiconductors [40]. This trend reflects that, in more disordered systems, a relatively larger fraction of the current is carried by states that are further away from the Fermi energy. That is, transitions where both the initial and final hopping states lie close to E_F are less relevant to the percolating network and contribute less to conductivity than in a band conductor.

In Fig. 6, the calculated thermoelectric figure of merit, zT, is plotted, using the same network parameters as those
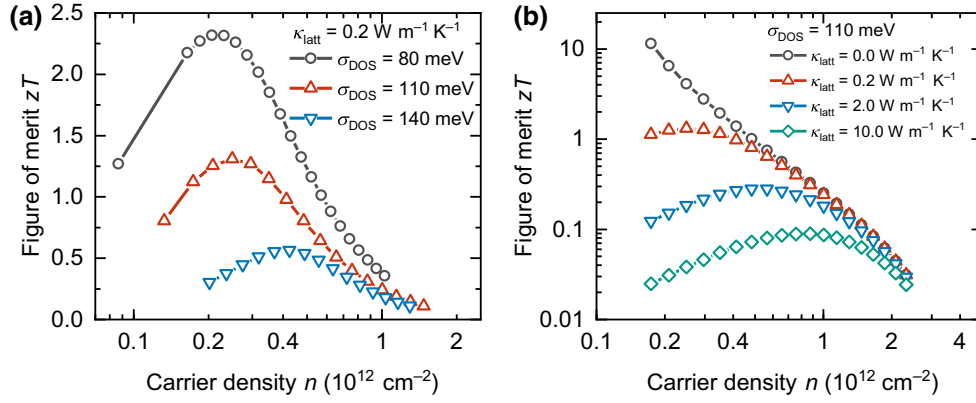
FIG. 6.   Calculated thermoelectric figure of merit versus charge density (a), parametric in energetic disorder, and lattice thermal conductivity (b). Calculation parameters are $\beta = 4.3$, $l_d = 12.6\ \mu\mathrm{m}^{-1}$, and $l_0 = (0.95 \pm 0.4)\ \mu\mathrm{m}$.

for the simulation of the (6,5) SWCNT network data in Fig. 4. Since the calculation of zT requires a 3D conductance, while the model is (so far) set up for quasi-2D systems, we transform the 2D conductivity into a 3D one by dividing by twice the tube diameter as a typical maximum active-layer thickness. For finite values of κ_latt, the figure of merit shows the common trade-off between increasing conductivities and decreasing Seebeck coefficient, leading to a maximum at intermediate carrier densities; in the absence of lattice thermal conductivity, the thermal and electronic conductivities essentially cancel out, and zT follows the decreasing Seebeck coefficient with increasing conductivity and carrier density.

Unsurprisingly, the maximum figure of merit decreases with increasing energetic disorder and lattice thermal conductivity. More interesting are the relatively large absolute values that are obtained, even for relatively large values of $\kappa_\mathrm{latt} \approx 2\ \mathrm{W\,m}^{-1}\mathrm{K}^{-1}$. Unfortunately, no consistent picture arises in the literature about the actual values of κ_latt in SWCNT networks, with reported values ranging from around $0.1\ \mathrm{W\,m}^{-1}\mathrm{K}^{-1}$ to above $10\ \mathrm{W\,m}^{-1}\mathrm{K}^{-1}$ [5,50,51]. If we consider an intermediate value of $\kappa_\mathrm{latt} \approx 2\ \mathrm{W\,m}^{-1}\mathrm{K}^{-1}$, Fig. 6 shows that zT can go significantly beyond 0.2, suggesting there is considerable room for improvement over the reported value of $zT \approx 0.03$ around room temperature [52]. Further increases in zT can potentially be realized by suppressing energetic disorder or by tailoring the thermal coupling between the tubes by, for example, polymer wrapping.

Finally, it should be borne in mind that κ_latt might vary with energetic disorder. While charge impurities are not likely to affect the propagation of vibrations or phonons, other sources of energetic disorder might do so. In general, κ_latt should be reduced with increasing energetic disorder as the system is more prone to scattering of propagating quasi-particles (charges, phonons). Hence, the lines in Fig. 6 are to be considered as orthogonal projections of a multidimensional parameter space and provide a range and trends for the experimentally reachable figures of merit for a plausible range of parameters.

IV. CONCLUSION

We present a model for the charge and energy transport in random quasi-2D SWCNT networks. The network properties are calculated as a random resistor network, in which both the intra- and intertube resistances are accounted for. A consistent fit to experimental conductivity and Seebeck coefficient data over a wide range of temperature and carrier concentrations requires the inclusion of significant, i.e., several times the thermal energy, energetic disorder. Extending the model to the electronic contribution to the thermal conductivity leads, for low-disorder networks, to κ_el values that are close to the predictions from the Wiedemann-Franz law for band-type transport. For more disordered networks, Lorentz factors that significantly exceed L_0 are found. For a realistic value of the lattice thermal conductivity, $\kappa_\mathrm{latt} = 2\ \mathrm{W\,m}^{-1}\mathrm{K}^{-1}$, the model indicates that a thermoelectric figure of merit of $zT > 0.2$ should be realistically achievable, while $zT > 1$ should be reachable for $\kappa_\mathrm{latt} = 0.2\ \mathrm{W\,m}^{-1}\mathrm{K}^{-1}$, which will require suppressing the thermal coupling between individual tubes and/or reducing the energetic disorder in the system.

[1] L. D. Hicks and M. S. Dresselhaus, Thermoelectric figure of merit of a one-dimensional conductor, Phys. Rev. B **47**, 16631 (1993).

[2] L. D. Hicks and M. S. Dresselhaus, Effect of quantum-well structures on the thermoelectric figure of merit, Phys. Rev. B **47**, 12727 (1993).

[3] J. W. Mintmire and C. T. White, Electronic and structural properties of carbon nanotubes, Carbon **33**, 893 (1995).

[4] N. T. Hung, A. R. T. Nugraha, E. H. Hasdeo, M. S. Dresselhaus, and R. Saito, Diameter dependence of thermoelectric power of semiconducting carbon nanotubes, Phys. Rev. B **92**, 165426 (2015).

[5] A. D. Avery, B. H. Zhou, J. Lee, E.-S. Lee, E. M. Miller, R. Ihly, D. Wesenberg, K. S. Mistry, S. L. Guillot, B. L. Zink, *et al.*, Tailored semiconducting carbon nanotube networks with enhanced thermoelectric properties, Nat. Energy **1**, 16033 (2016).

[6] I. Puchades, C. C. Lawlor, C. M. Schauerman, A. R. Bucossi, J. E. Rossi, N. D. Cox, and B. J. Landi, Mechanism of chemical doping in electronic-type-separated single wall carbon nanotubes towards high electrical conductivity, J. Mater. Chem. C **3**, 10256 (2015).

[7] B. Kumanek, K. Z. Milowska, Ł Przypis, G. Stando, K. Matuszek, D. MacFarlane, M. C. Payne, and D. Janas, Doping engineering of single-walled carbon nanotubes by nitrogen compounds using basicity and alignment, ACS Appl. Mater. Interfaces **14**, 25861 (2022).

[8] S. P. Schießl, N. Fröhlich, M. Held, F. Gannott, M. Schweiger, M. Forster, U. Scherf, and J. Zaumseil, Polymer-sorted semiconducting carbon nanotube networks for high-performance ambipolar field-effect transistors, ACS Appl. Mater. Interfaces **7**, 682 (2015).

[9] G. J. Brady, A. J. Way, N. S. Safron, H. T. Evensen, P. Gopalan, and M. S. Arnold, Quasi-ballistic carbon nanotube array transistors with current density exceeding Si and GaAs, Sci. Adv. **2**, e1601240 (2016).

[10] P. Sheng, Fluctuation-induced tunneling conduction in disordered materials, Phys. Rev. B **21**, 2180 (1980).

[11] M. E. Itkis, A. Pekker, X. Tian, E. Bekyarova, and R. C. Haddon, Networks of semiconducting SWNTs: Contribution of midgap electronic states to the electrical transport, Acc. Chem. Res. **48**, 2270 (2015).

[12] K. Yanagi, H. Udoguchi, S. Sagitani, Y. Oshima, T. Takenobu, H. Kataura, T. Ishida, K. Matsuda, and Y. Maniwa, Transport mechanisms in metallic and semiconducting single-wall carbon nanotube networks, ACS Nano **4**, 4027 (2010).

[13] L. Hu, D. S. Hecht, and G. Grüner, Percolation in transparent and conducting carbon nanotube networks, Nano Lett. **4**, 2513 (2004).

[14] X. Tian, M. L. Moser, A. Pekker, S. Sarkar, J. Ramirez, E. Bekyarova, M. E. Itkis, and R. C. Haddon, Effect of atomic interconnects on percolation in single-walled carbon nanotube thin film networks, Nano Lett. **14**, 3930 (2014).

[15] S. Tripathy, B. Bose, P. P. Chakrabarti, and T. K. Bhattacharyya, Resistive analysis of scattering-dependent electrical transport in single-wall carbon-nanotube networks, IEEE Trans. Electron Devices **67**, 5676 (2020).

[16] S. P. Schießl, X. De Vries, M. Rother, A. Massé, M. Brohmann, P. A. Bobbert, and J. Zaumseil, Modeling carrier density dependent charge transport in semiconducting carbon nanotube networks, Phys. Rev. Mater. **1**, 046003 (2017).

[17] M. Statz, S. Schneider, F. J. Berger, L. Lai, W. A. Wood, M. Abdi-Jalebi, S. Leingang, H.-J. Rg Himmel, J. Zaumseil, and H. Sirringhaus, Charge and thermoelectric transport in polymer-sorted semiconducting single-walled carbon nanotube networks, ACS Nano **14**, 15552 (2020).

[18] D. Enfin and C. G. Kuper, Breakdown of the resistor-network model for steady-state hopping conduction, Czech. J. Phys. **46**, 2431 (1996).

[19] S. Datta, Exclusion principle and the Landauer-Büttiker formalism, Phys. Rev. B **45**, 1347 (1992).

[20] M. Stadermann, S. J. Papadakis, M. R. Falvo, J. Novak, E. Snow, Q. Fu, J. Liu, Y. Fridman, J. J. Boland, R. Superfine, *et al.*, Nanoscale study of conduction through carbon nanotube networks, Phys. Rev. B **69**, 201402 (2004).

[21] P. N. Nirmalraj, P. E. Lyons, S. De, J. N. Coleman, and J. J. Boland, Electrical connectivity in single-walled carbon nanotube networks, Nano Lett. **9**, 3890 (2009).

[22] F. Bottacchi, S. Bottacchi, F. Späth, I. Namal, T. Hertel, and T. D. Anthopoulos, Nanoscale charge percolation analysis in polymer-sorted (7,5) single-walled carbon nanotube networks, Small **12**, 4211 (2016).

[23] S. Colasanti, V. Deep Bhatt, A. Abdelhalim, and P. Lugli, 3-D percolative model-based multiscale simulation of randomly aligned networks of carbon nanotubes, IEEE Trans. Electron Devices **63**, 1346 (2016).

[24] A. Javey, J. Guo, Q. Wang, M. Lundstrom, and H. Dai, Ballistic carbon nanotube field-effect transistors, Nature **424**, 654 (2003).

[25] M. S. Fuhrer, J. Nygård, L. Shih, M. Forero, Y.-G. Yoon, M. S. C. Mazzoni, H. J. Choi, J. Ihm, S. G. Louie, A. Zettl, *et al.*, Crossed nanotube junctions, Science **288**, 494 (2000).

[26] M. A. Topinka, M. W. Rowell, D. Goldhaber-Gordon, M. D. McGehee, D. S. Hecht, and G. Gruner, Charge transport in interpenetrating networks of semiconducting and metallic carbon nanotubes, Nano Lett. **9**, 1866 (2009).

[27] R. Saito and G. Dresselhaus, Trigonal warping effect of carbon nanotubes, Phys. Rev. B **61**, 2981 (2000).

[28] See the Supplemental Material at http://link.aps.org/supplemental/10.1103/PhysRevApplied.18.064022 for further calculations and fits to experimental data as well as an illustration of the model.

[29] T. Filleter and H. D. Espinosa, Multi-scale mechanical improvement produced in carbon nanotube fibers by irradiation cross-linking, Carbon **56**, 1 (2013).

[30] M. C. J. M. Vissenberg and M. Matters, Theory of the field-effect mobility in amorphous organic transistors, Phys. Rev. B **57**, 12964 (1998).

[31] V. Ambegaokar, B. I. Halperin, and J. S. Langer, Hopping conductivity in disordered systems, Phys. Rev. B **4**, 2612 (1971).

[32] J. Cottaar, L. J. A. Koster, R. Coehoorn, and P. A. Bobbert, Scaling Theory for Percolative Charge Transport in Disordered Molecular Semiconductors, Phys. Rev. Lett. **107**, 136601 (2011).

[33] A. Miller and E. Abrahams, Impurity conduction at low concentrations, Phys. Rev. **120**, 745 (1960).

[34] B. Movaghar, B. Pohlman, and W. Schirmacher, Random walk in disordered hopping systems, Solid State Commun. **34**, 451 (1980).

[35] E. Castaño and G. Kirczenow, Numerical study of ballistic conduction through a constriction with a barrier, Solid State Commun. **70,** 801 (1989).

[36] X. Zhou, J. Y. Park, S. Huang, J. Liu, and P. L. McEuen, Band Structure, Phonon Scattering, and the Performance Limit of Single-Walled Carbon Nanotube Transistors, Phys. Rev. Lett. **95,** 146805 (2005).

[37] S. Datta, *Electronic Transport in Mesoscopic Systems* (Cambridge university press, Cambridge, 1997).

[38] G. Pennington and N. Goldsman, Semiclassical transport and phonon scattering of electrons in semiconducting carbon nanotubes, Phys. Rev. B **68,** 045426 (2003).

[39] H. Fritzsche, A general expression for the thermoelectric power, Solid State Commun. **9,** 1813 (1971).

[40] D. Scheunemann and M. Kemerink, Non-Wiedemann-Franz behavior of the thermal conductivity of organic semiconductors, Phys. Rev. B **101,** 75206 (2020).

[41] D. Scheunemann and M. Kemerink, in *Organic Flexible Electronics*, edited by P. Cosseddu and M. Caironi (Elsevier, Amsterdam, 2021), p. 165.

[42] S. D. Baranovskii, Theoretical description of charge transport in disordered organic semiconductors, Phys. Status Solidi B **251,** 487 (2014).

[43] S. D. Baranovskii, T. Faber, F. Hensel, and P. Thomas, The applicability of the transport-energy concept to various disordered materials, J. Phys.: Condens. Matter **9,** 2699 (1997).

[44] J. Ziman, *Electrons and Phonons: The Theory of Transport Phenomena in Solids* (Oxford university press, New York, 2001).

[45] K. Xu, T. Ruoko, M. Shokrani, D. Scheunemann, H. Abdalla, H. Sun, C. Yang, Y. Puttisong, N. B. Kolhe, J. S. M. Figueroa, *et al.*, On the origin of Seebeck coefficient inversion in highly doped conducting polymers, Adv. Funct. Mater. **32,** 2112276 (2022).

[46] W. F. Pasveer, J. Cottaar, C. Tanase, R. Coehoorn, P. A. Bobbert, P. W. M. Blom, D. M. de Leeuw, and M. A. J. Michels, Unified Description of Charge-Carrier Mobilities in Disordered Semiconducting Polymers, Phys. Rev. Lett. **94,** 206601 (2005).

[47] M. Rother, M. Brohmann, S. Yang, S. B. Grimm, S. P. Schießl, A. Graf, and J. Zaumseil, Aerosol-jet printing of polymer-sorted (6, 5) carbon nanotubes for field-effect transistors with high reproducibility, Adv. Electron. Mater. **3,** 1700080 (2017).

[48] W. S. C. Roelofs, S. G. J. Mathijssen, R. A. J. Janssen, D. M. De Leeuw, and M. Kemerink, Accurate description of charge transport in organic field effect transistors using an experimentally extracted density of states, Phys. Rev. B **85,** 085202 (2012).

[49] T. Richards, M. Bird, and H. Sirringhaus, A quantitative analytical model for static dipolar disorder broadening of the density of states at organic heterointerfaces, J. Chem. Phys. **128,** 234905 (2008).

[50] B. A. Macleod, N. J. Stanton, I. E. Gould, D. Wesenberg, R. Ihly, Z. R. Owczarczyk, K. E. Hurst, C. S. Fewox, C. N. Folmar, K. Holman Hughes, *et al.*, Large *n*- and *p*-type thermoelectric power factors from doped semiconducting single-walled carbon nanotube thin films, Energy Environ. Sci. **10,** 2168 (2017).

[51] R. S. Prasher, X. J. Hu, Y. Chalopin, N. Mingo, K. Lofgreen, S. Volz, F. Cleri, and P. Keblinski, Turning Carbon Nanotubes from Exceptional Heat Conductors into Insulators, Phys. Rev. Lett. **102,** 105901 (2009).

[52] D. J. Wesenberg, M. J. Roos, A. D. Avery, J. L. Blackburn, A. J. Ferguson, and B. L. Zink, Size- and temperature-dependent suppression of phonon thermal conductivity in carbon nanotube thermoelectric films, Adv. Electron. Mater. **6,** 2000746 (2020).